*16th World Conference on Earthquake Engineering, 16WCEE 2017*
*Santiago Chile, January 9th to 13th 2017*
*Paper N° 1220*
*Registration Code: S-U1473984633*

# Quantitative Estimation of Basin Effects Based on Statistical Analysis

C. Zhu[(1)], D. Thambiratnam[(2)] , J. Zhang[(3)] and C. Gallage[(4)]

[(1)] *PhD Candidate, School of Civil Engineering and the Built Environment, Queensland University of Technology, Australia,* c2.zhu@qut.edu.au
[(2)] *Professor, School of Civil Engineering and the Built Environment, Queensland University of Technology, Australia,* d.thambiratnam@qut.edu.au
[(3)] *Professor, School of Civil Engineering, Southwest Jiaotong University, China,* jianzhang1102@home.swjtu.edu.cn
[(4)] Senior Lecturer, *School of Civil Engineering and the Built Environment, Queensland University of Technology, Australia,* chaminda.gallage@qut.edu.au

## *Abstract*

Basin effects have been proven to be of significance to seismic ground motion by many researchers, yet 1D site response analysis, especially based on equivalent nonlinear method, has been dominating in engineering practice. With the aim of contributing to the incorporation of complex site effects into seismic provisions, quantification of 2D basin effects for shallow basins is conducted in this research based on statistics-based numerical analysis to a total of 50 vertically heterogeneous basin configurations subject to real earthquakes recorded on rock sites across the world. It is concluded that for a shallow basin, calibration to the acceleration spectra is only needed to locations within the close-to-edge region of which the width is linear correlated to the basin depth by a factor between 1.2 and 1.5.

*Keywords: site effects, basin, 2D, surface waves, statistics*

## 1. Introduction

Researchers have observed and then recognised the basin effects as the topographical, geotechnical and geophysical effect of superficial soil layers on strong ground motion (Hanks, 1975; Tucker and King, 1984; King and Tucker, 1984; Bard and Bouchon, 1980a,b) for several decades. Basin effects have received much attention as they not only involve spatially varying and elongated ground motion as well as anomalous amplification, but also because of the fact that many urban areas in the world, such as Los Angeles, Tokyo, Osaka and Kathmandu, are situated atop alluvial basin configurations.

Numerous studies on basin effects have thus been conducted by means of both theoretical methods (Aki and Larner, 1970; Trifunac, 1971; Wong and Trifunac, 1974; Bard and Bouchon, 1980a, b; Sánchez-Sesma et al., 1993; Paolucci, 1999; Faccioli and Vanini, 2003; Chávez-García, 2003; Stamati et al., 2016; among many others) and field tests (Pitilakis, 1999; Kawase and Sato, 1992; Field, 1996; Raptakis et al., 2004; Makra and Chávez-García, 2016; among others).

These studies contribute to the understanding of the underpinning mechanisms and the features exclusive to multidimensional basin effects, including (a) 2D resonance (Bard and Bouchon, 1985; Rail and Ling, 1992; Roten et al., 2006; Ermert et al., 2014, among many others); (b) Surface waves (Bard and Bouchon, 1980a, b; Moczo and Bard, 1993; Chávez-García, 1994; Kawase, 1996; Raptakis, et al., 2004; Makra et al., 2016; Zhu et al., 2015; Zhu and Thambiratnam, 2016, among many others); (c) Other wave phenomena due to the multidimensional geometries, such as focusing effect (Hudson, 1963; Ishii and Ellis, 1970a and b; Sánchez-Sesma and Velazquez, 1987; Gao et al., 1996; Ktenidou, et al., 2016, among many others).

Although the mechanism of the multi-dimensional site effects have long been clarified, modern seismic regulations are still mainly based on 1D assumptions which has proved to be unable to reproduce the ground motions of some basins where basin effects need to be taken into account (Chávez-García, 1994; Chávez-García and Faccioli, 2000; Smerzini et al., 2011; Makra and Chávez-García, 2016; Kristel, 2016). To contribute to the eventual incorporation of the multi-dimensional site effects into seismic codes, a quantitative estimation to the basin effects is necessary. Given the uncertain nature of this problem, a statistical study is needed to provide a compelling result. Therefore, a statistics-based quantitative study on basin effects are carried out in this research in order to quantify the multi-dimensional site effects.

In order to quantify basin effects, some researchers tried to introduce basin depth into ground motion attenuation model through the analysis of strong ground motion data (Trifunac and Lee, 1978, Campbell, 1997; Field, 2000; Lee and Anderson, 2000; Jorner, 2000; Somerville, 2004; Hruby and Bersnev, 2003; Choi et al., 2005).

Chávez-García and Faccioli (2000) explored a different way by introducing an “aggravation factor” (*AG*) which is defined as the ratio between response spectra computed at the surface of the 2D model and the response spectra computed at the surface of the equivalent 1D model to quantify the additional the additional amplification or de-amplification caused by basin effects, thus bridging the gap between 1D and multi-dimensions (Faccioli and Vanini, 2003; Raptakis et al., 2004; Makra et al., 2005; Vessi and Russo, 2013; Pitilakis et al., 2015; Riga, 2015).

Based on the aggravation factor proposed by Chávez-García and Faccioli (2000), a more comprehensive gauge - Spectral Aggravation factor (*SAG*), was introduced in our previous studies (Zhu and Thambiratnam, 2016) to account for both the frequency and spatiality dependency of *AG*:

$$SAG(T/T_0,\ x/L) = \frac{SA_{2D}(T/T_0,\ x/L)}{SA_{1D}(T/T_0,\ x/L)} \tag{1}$$

where $SA_{2D}\,(T/T_0,\ x/L)$ and $SA_{1D}\,(T/T_0,\ x/L)$ - spectral acceleration (*SA*) at receiver $x/L$ of 2D model and its corresponding 1D model respectively, *x*- distance of a surface point from the basin centre; *L*- basin half-width; *T*- spectral period, $T_0$- fundamental frequency of the equivalent plane layers of a basin by weighted average method. The present research aims to provide a statistical value of *SAG*.

## 2. Numerical modelling

There exist only a very few basins or valleys to which both detailed information on geometry as well as dynamic property and high-quality strong ground motions are available, which renders it significantly difficult, if not impossible, to conduct statistical study on strong ground motions recorded on a large enough number of real basins. Thus, numerical study on a large number of hypothetic basins is implemented in this study.

### 3.1 Modelling method

Seismic response of a basin is simulated by an explicit FD (finite difference) code- 2DFD_DVS developed by Moczo et al. (2004, 2007) and Kristek (2002, 2003). This FD method solves the equations of motion in the 2D heterogeneous isotropic viscoelastic structures with a planar free surface. The scheme is 4th-order accurate in space and 2nd-order accurate in time. The computational region is an area of a rectangle with the bottom, left and right sides representing non-reflecting boundaries. Upper cut-off frequency $f_{cut}$ is set to 10 Hz, and correspondingly, the spatial step is one tenth of the minimum wavelength (Kuhlemeyer and Lysmer, 1973) to balance the numerical efficiency and accuracy.

The critical time step of the dynamic analysis is set to satisfy the stability condition for the 4th-order staggered grid FD scheme based on the spatial step and maximum *P*-wave velocity of the model:

$$\Delta t \leq \frac{6h}{7\sqrt{2}v_p} \tag{2}$$

where h is the grid spacing, and $v_p$ is the compressional wave velocity.

The rheology of the medium corresponds to the generalised Maxwell body, which makes it possible to guarantee the quality factor ($Q$) variable for different materials but constant within the frequency range of interest. Quality factor for shear ($Q_s$) and compressional ($Q_p$) waves are defined as:

$$Q_s = v_s/10 \tag{3}$$

$$Q_p = 2Q_s \tag{4}$$

where $Q_s$ and $Q_p$ - quality factor for shear and compressional waves respectively; *vs* - shear wave velocity. The code also allows 1D simulation for local 1D model defined by the distribution of material parameters along each vertical grid line. Thus, 1D computations are also realized by the same code. This technique was thoroughly verified in details by Makra et al. (2012) and Riga (2015).

### 3.2 Basin configurations

Previous researches show that seismic ground motion of shallow basins is dominated by the propagation of surface waves initiated at basin edges, triggering intense ground motion in the close-to-edge areas, while for deep basins, 2D resonance will be dominant, mobilising the whole basin (Bard and Bouchon, 1985). Since shallow basins present a different ground motion pattern from deep basins when subjected to seismic motion, only shallow basins are studied in the present research.

Based on a preliminary study on several real basin geometries (Sanchez-Sesma, 1988; Raptakis et al., 2000; Kawase and Sato, 1992; Kato et al., 1993; Graves , 1993; Gao, 1996; Olsen, 2000; Satoh, 2001; Adams, 2003; Takao, 2004; Lacave and Lemeille, 2006; Roten, 2008; Miksat, 2010; Gelagoti, 2010; Shani-Kadmiel, 2012; Srinagesh, 2011; Kham, 2013; Ragozzino, 2014; Giulio et al., 2016), a generic shallow basin configuration (Fig. 1) is proposed, a symmetrical trapezoidal shape with constant basin half-width $L$=2500 m, to guarantee that all the basins are broad enough so as to eliminate the possibility of 2D resonance (Bard and Bouchon, 1985) without compromising the generality of the basin geometry from an engineering practice perspective.

According to our previous study (Zhu and Thambiratnam, 2016), only when the incident wavelength is smaller than the depth of a basin, can the incident angle $\alpha$ manifest its implication on basin ground motion, namely wedge effect which is defined as the wave-trapping effect in small-angled wedge (AF=1.0 or so in the edge areas) or wave-deflecting effect in large-angled wedge (AF<1.0 in the edge areas). Thus slope angle $\alpha$ is fixed to $45^0$ in the present study.

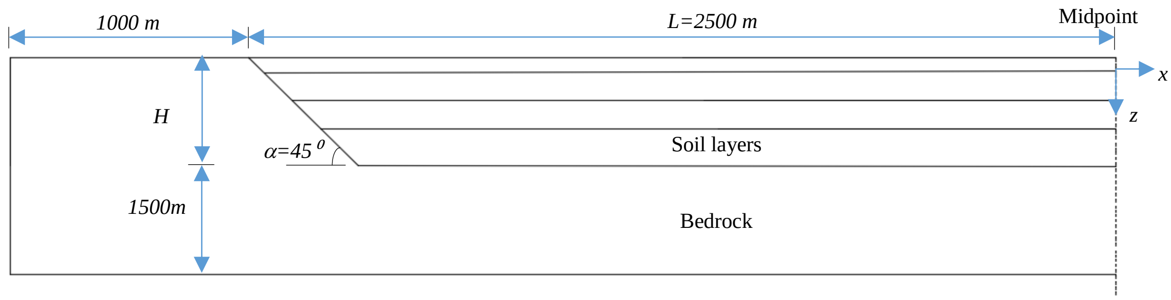


**Fig. 1** Schematic diagram of FD model (only half of the model is displayed because of symmetry)

A total of 50 hypothetic shallow basins with constant $L$ and $\alpha$ (Table 1) are configured with vertical inhomogeneity. Among them, 31 basin models are configured based on real 1D soil profiles (Table 2) compiled from KiK-net database. Another 19 2D configurations are constructed based on hypothetic 1D profile in order to achieve a set of basins well distributed in the $H(v_s$=800)-$v_{s,30}$ chart, as shown in Fig. 2. In Fig. 2, ***H*(*v_s*=800)** presents the depth to the layer with shear wave velocity greater than 800 m/s and $\boldsymbol{v_{s,30}}$ is the average shear wave velocity of the topmost soil layers within 30m.

The lateral boundaries of the FD model are placed 1000m away from the corresponding basin edges, while the horizontal boundary is set 1500m below the bottom of the basin (Fig. 1), to minimise the influence of any possible boundary reflections. Receivers are evenly distributed along the basin surface with an interval of 20 m.

### 3.3 Input motions

A total of nine strong ground motions (Table 3) recorded on bedrock site ($v_{s,30}$ >760 m/s) are selected from the *Pacific Earthquake Engineering Research Centre Strong Ground Motion Database* and input at the model base as vertically incident *SH* waves. All these seismic records are baseline-corrected as well as bandpass-filtered with cut-off frequencies of 0.2 and 10.0 Hz.. The acceleration response spectra of these input motions are depicted in Fig. 3, which shows that these excitations are compatible with the spectra recommended for rock site in *Eurocode 8*. Each basin models are excited by these nine records. *SAG (T, x/L)* is then averaged over the nine incidences, and the average *SAG* $(T/T_0, x/L)$ is referred to as $\overline{SAG}$ $(T/T_0, x/L)$:

$$\overline{SAG}\left(T/T_0,\ x/L\right)=\frac{\sum_{i=1}^{9}SAG(T/T_0,\ x/L)}{9} \tag{5}$$

where $\overline{SAG}$ $(T/T_0, x/L)$ is the mean of the *SAG*s of the nine excitations.

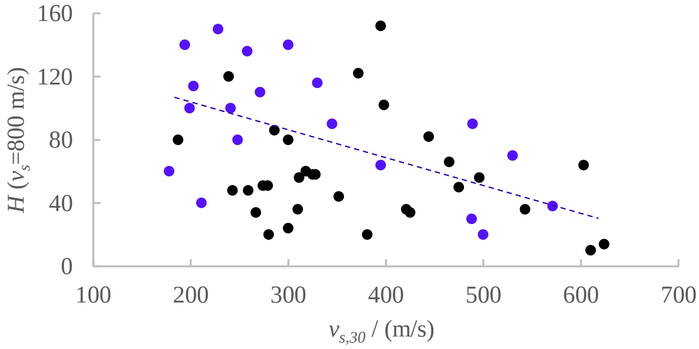


**Fig. 2** $H$ ($v_s$=800 m/s) vs. $v_{s,30}$ at the centre ($x/L$=0) of all basins. $H$ ($v_s$=800 m/s) is the depth to the top of the first layer with shear wave velocity greater than 800 m/s, and $v_{s,30}$ is the average shear wave velocity of the topmost soil layers within 30m.

Blue dots are basins configured from hypothetic 1D profile; Black dots are basins configured on real 1D profile from KiK-net;

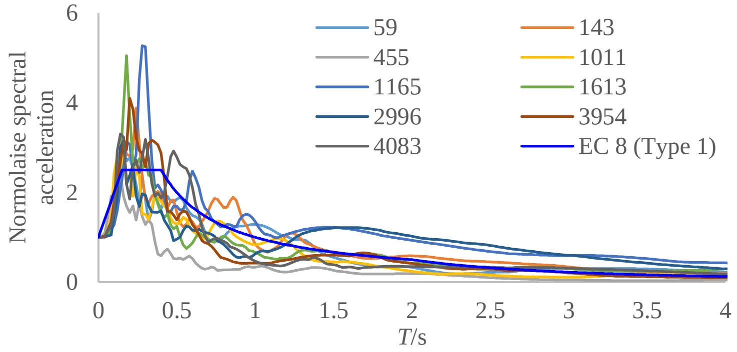


**Fig. 3** Acceleration response spectra (5% damping) of input motions

**Table 1** Vertically inhomogeneous basin models configured from 1D soil profiles

| No. | Type | KiK-net Code | $v_{s,30}$ | $H$ ($v_s$=800) | Type | KiK-net Code | $v_{s,30}$ | $H$ ($v_s$ =800) |
|---|---|---|---|---|---|---|---|---|
| 1 | | AICH16 | 352 | 44 | | ABSH05 | 624 | 14 |
| 2 | | EHMH09 | 267 | 34 | | ABSH10 | 610 | 10 |
| 3 | | FKIH04 | 300 | 80 | | KGSH01 | 603 | 64 |
| 4 | | FKIH05 | 187 | 80 | | RMIH04 | 543 | 36 |
| 5 | | GIFH06 | 300 | 24 | | KOCH12 | 496 | 56 |
| 6 | | HRSH06 | 279 | 51 | | AKTH01 | 475 | 50 |
| 7 | | HYGH11 | 274 | 51 | | ABSH15 | 465 | 66 |
| 8 | | IBUH07 | 259 | 48 | | ISKH04 | 444 | 82 |
| 9 | | KKWH10 | 328 | 58 | | SMNH03 | 425 | 34 |
| 10 | | KKWH11 | 243 | 48 | | GNMH11 | 421 | 36 |
| 11 | | NGNH32 | 310 | 36 | B | YMTH10 | 398 | 102 |
| 12 | | NIGH18 | 311 | 56 | | AICH14 | 395 | 152 |
| 13 | | OSMH01 | 239 | 120 | | NGSH05 | 381 | 20 |
| 14 | | SBSH08 | 325 | 58 | | YMTH07 | 372 | 122 |
| 15 | C | SMNH07 | 318 | 60 | | MB1 | 488 | 30 |
| 16 | | SRCH02 | 280 | 20 | | MB2 | 530 | 70 |
| 17 | | YMTH15 | 286 | 86 | | MB3 | 395 | 64 |
| 18 | | MC1 | 345 | 90 | | MB4 | 489 | 90 |
| 19 | | MC2 | 199 | 100 | | MB5 | 500 | 20 |
| 20 | | MC3 | 271 | 110 | | MB6 | 571 | 38 |
| 21 | | MC4 | 248 | 80 | | | | |
| 22 | | MC5 | 300 | 140 | | | | |
| 23 | | MC6 | 178 | 60 | | | | |
| 24 | | MC7 | 211 | 40 | | | | |
| 25 | | MC8 | 241 | 100 | | | | |
| 26 | | MC9 | 194 | 140 | | | | |
| 27 | | MC10 | 228 | 150 | | | | |
| 28 | | MC11 | 330 | 116 | | | | |
| 29 | | MC12 | 258 | 136 | | | | |
| 30 | | MC13 | 203 | 114 | | | | |

**Table 2** Soil profile of OSMH01 from KiK-net

| | Thickness (m) | Depth (m) | $v_p$ (m/s) | $v_s$ (m/s) |
|---|---|---|---|---|
| 1 | 6 | 6 | 430 | 180 |
| 2 | 10 | 16 | 1570 | 180 |
| 3 | 14 | 30 | 2430 | 380 |
| 4 | 16 | 46 | 1750 | 280 |
| 5 | 74 | 120 | 1750 | 580 |
| Bedrock | ----- | ----- | 2070 | 900 |

**Table 3** List of earthquake records used as vertically incident *SH* waves

| Record Number | Earthquake | Year | Station Name | Magn. | Rrup. (km) | $v_{s,30}$ (m/sec) |
|---|---|---|---|---|---|---|
| 59 | "San Fernando" | 1971 | "Cedar Springs Allen Ranch" | 6.6 | 89.72 | 813.48 |
| 143 | "Tabas Iran" | 1978 | "Tabas" | 7.4 | 2.05 | 766.77 |
| 455 | "Morgan Hill" | 1984 | "Gilroy Array #1" | 6.2 | 14.91 | 1428.14 |
| 1011 | "Northridge-01" | 1994 | "LA - Wonderland Ave" | 6.7 | 20.29 | 1222.52 |
| 1165 | "Kocaeli Turkey" | 1999 | "Izmit" | 7.5 | 7.21 | 811.00 |
| 1613 | "Duzce Turkey" | 1999 | "Lamont 1060" | 7.1 | 25.88 | 782.00 |
| 2996 | "Chi-Chi Taiwan-05" | 1999 | "HWA003" | 6.2 | 50.44 | 1525.85 |
| 3954 | "Tottori Japan" | 2000 | "SMNH10" | 6.6 | 15.59 | 967.27 |
| 4083 | "Parkfield-02 CA" | 2004 | "PARKFIELD - TURKEY FLAT #1 (0M)" | 6.0 | 5.29 | 906.96 |

## 3. Results and analysis

Each of these 50 basin models (Table 1) are excited by the nine seismic records (Table 3) for both 1D and 2D scenarios. Thus, a total of 900 cases are simulated in this investigation. $\overline{SAG}$ *(T/T₀, x/L)s* are then derived for each of these 50 basin configurations.

### 4.1 $\overline{SAG}$ *(T/T0, x/L)*

$\overline{SAG}$ *($T/T_0$, x/L)s* of basin YMTH10, MB3, FKIH04 and MC1 are displayed in Fig. 4, which well exemplifies the multivariate nature of $\overline{SAG}$ *($T/T_0$, x/L)*, namely *$T/T_0$- x/l* dependence. It would be too onerous to be applicable if aggravation factor is variable with either different periods or locations. A more applicable indicator than $\overline{SAG}$ *($T/T_0$, x/L)* is thus to be explored.

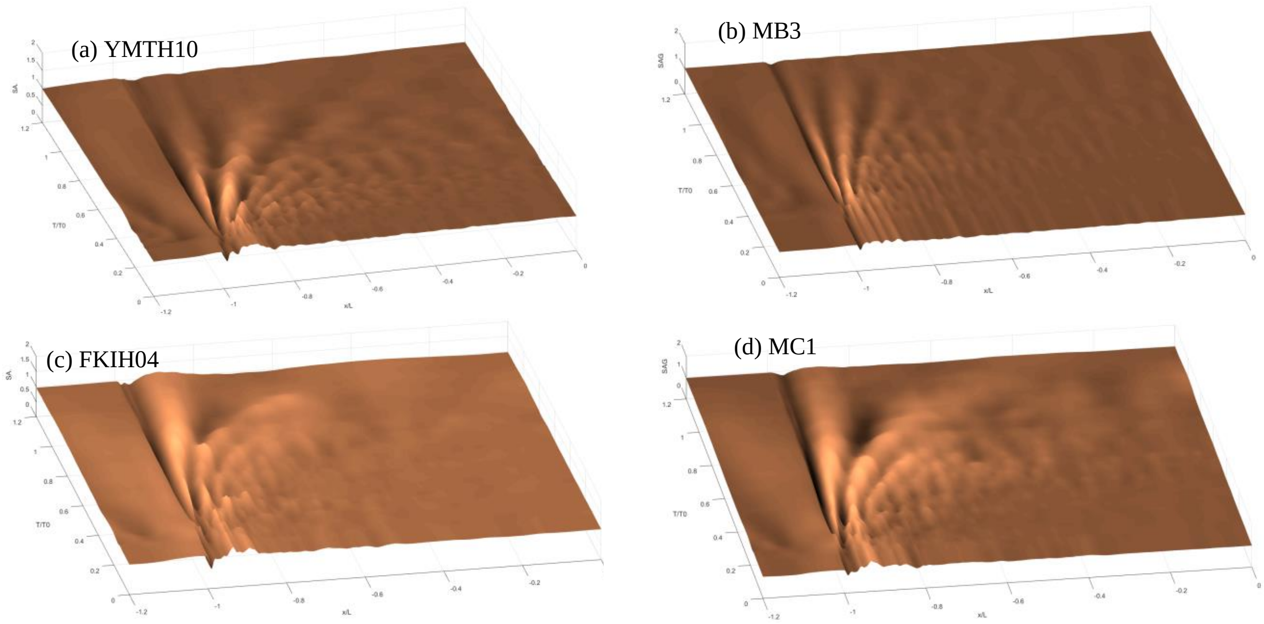


**Fig. 4** $\overline{SAG}$ *($T/T_0$, x/L)* of (a) YMTH10 (Type B); (b) MB3 (Type B); (c) FKIH04 (Type C); and (d) MC1 (Type C)

### 4.2 $\overline{SAG}$ *(x/L)*

Fig. 4 is re-presented in a 2D chart as shown in Fig. 5. It can be observed from Fig. 5 that the 2D effect manifests itself only when $T \leq T_0$, regardless of location (*x/L*). The same pattern can also be observed from all the other basin configurations. Moreover, this observation is consistent with these of Chávez-García and Faccioli (2000) and Riga (2015) who draw the same conclusion in their respective study. It is thus reasonable to focus on structural periods no more than $T_0$. Accordingly, a new indicator is introduced - $\overline{SAG}$ *(x/L)*, which is the maximum value of $\overline{SAG}$ $(T/T_0, x/L)$ within $T \leq T_0$:

$$\overline{SAG}\left(x/L\right)=\max\left[\overline{SAG}\left(T/T_0\leq 1,\ x/L\right)\right] \tag{6}$$

$\overline{SAG}$ *(x/L)s* of model YMTH10, MB3, FKIH04 and MC1 are depicted in Fig. 6, with a schematic basin configuration presented below. Fig. 6 shows the spatial-dependence of the $\overline{SAG}$ *(x/L)*, which indicates that the 2D site effects influence different basin surface regions to different extents. The fact that the $\overline{SAG}$ *(x/L)* peaks in an area close to basin edge suggests that the implication of 2D effects is only limited to the close-to-edge region, and this is expected for shallow basins (Zhu and Thambiratnam, 2016).

$\overline{SAG}$ *(x/L)s* of all the Type B and C sites are shown in Fig. 7 (a) and (b) respectively, which illustrate the concentration of 2D effects. The maximum values of each $\overline{SAG}$ *(x/L)* curves shown in Fig. 7 (a) and (b) are depicted against $v_{s,30}$ and $H(v_s$=800 m/s) in Fig. 8 (a) and (b) respectively.

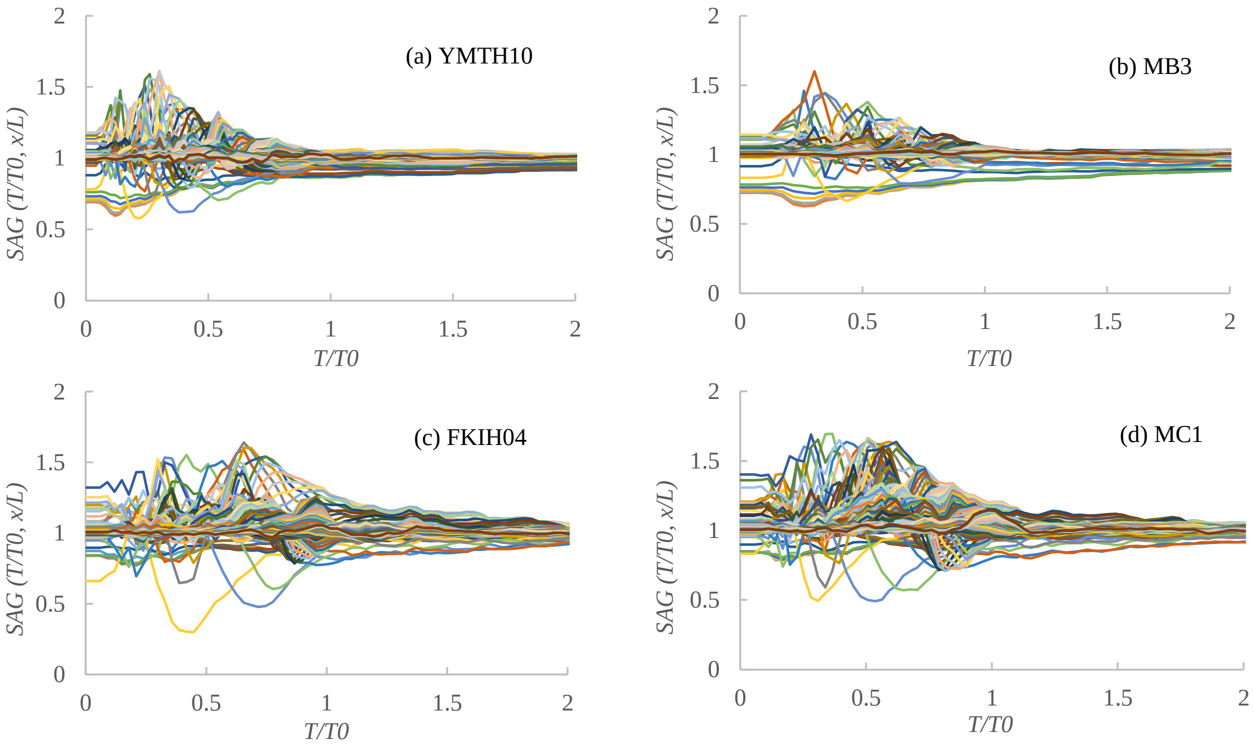


**Fig. 5** $\overline{SAG}$ *(T/T₀, x/L)* of (a) YMTH10 (Type B); (b) MB3 (Type B); (c) FKIH04 (Type C); and (d) MC1 (Type C)

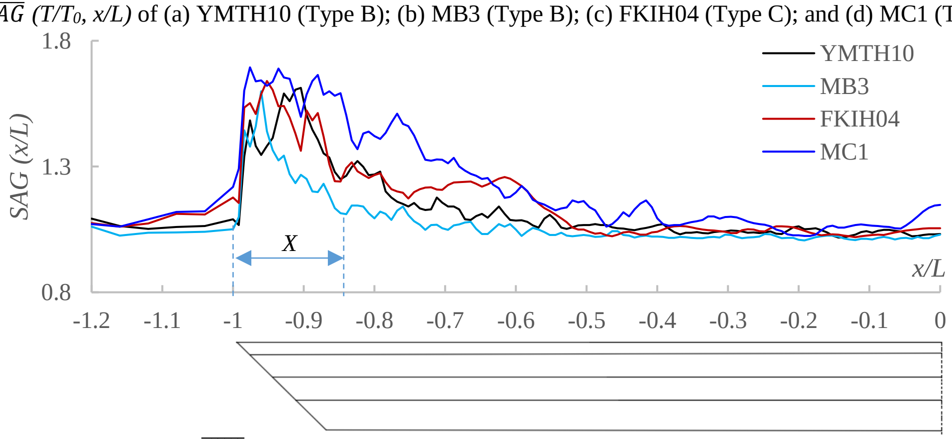


**Fig. 6** $\overline{SAG}(x/L)$ of basin model YMTH10, MB3, FKIH04 and MC1

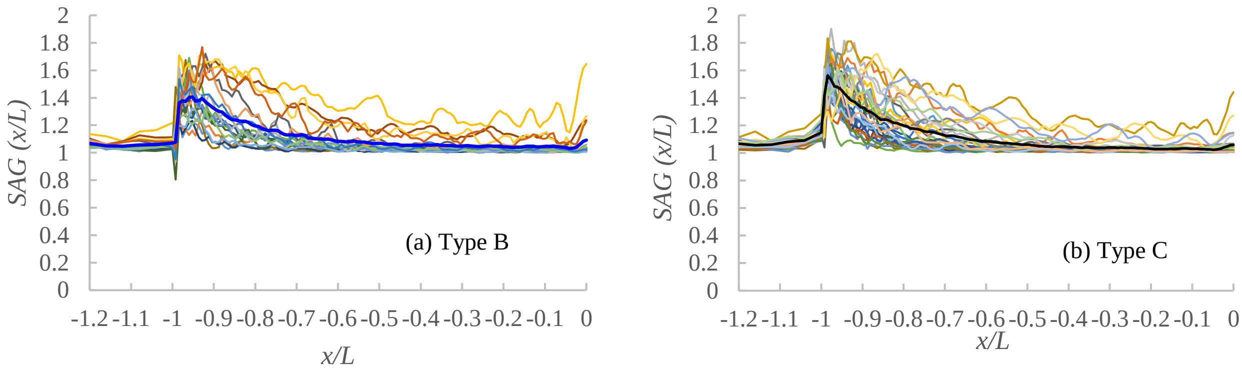


**Fig. 7** $\overline{SAG}(x/L)$ of all (a) Type B basins; and (b) Type C basins, and bold lines are the averages.

In comparison with Type C sites, a broader region of the Type B sites tend to be affected by 2D site effects (Fig. 7), which can be attributed to the generally higher attenuation of Type C sites than Type B sites. However, Type C sites tend to be of higher amplitude than C sites (Fig. 8a), which is in accordance with the conclusion that aggravation factor increases with the impedance ratio (Chávez-García and Faccioli, 2000; Riga, 2015). Fig. 8 also suggests that the maximum values of $\overline{SAG}$ *(x/L)* are less irrelevant to the *H* ($v_s$*=800 m/s*) than to $v_{s,30}$.

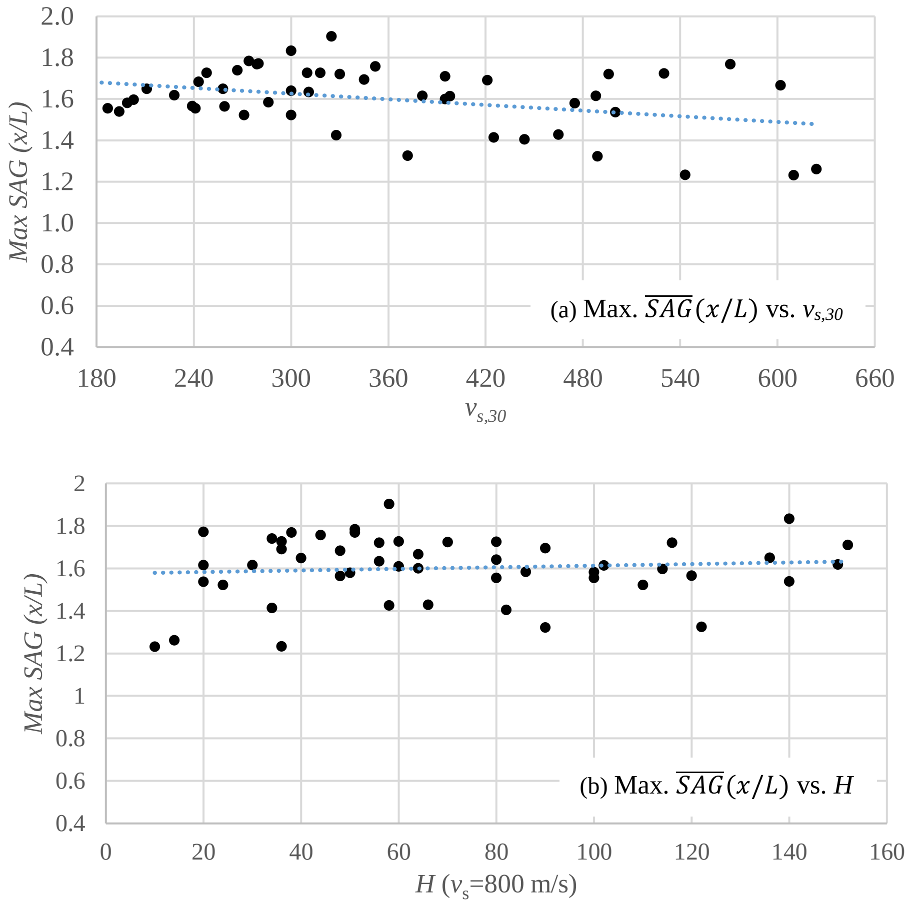


**Fig. 8** Maximum of $\overline{SAG}(x/L)$. (a) Max. $\overline{SAG}(x/L)$ vs. $v_{s,30}$; (b) Max. $\overline{SAG}(x/L)$ vs. *H* ($v_s$*=800 m/s)*. *H*($v_s$=800) denotes the depth of the top of the first layer with shear wave velocity greater than 800 m/s; $v_{s,30}$ is the average shear wave velocity of the topmost soil layers within 30m.

## 4.3 Influential area

The aim of this investigation is to contribute to the proposal of a reliable and applicable method to incorporate the 2D site effects into seismic provision via the aggravation factor. It would be considered to be over conservative to calibrate design spectral based on the maximum value of $\overline{SAG}$ *(x/L)* (Fig. 8). Furthermore, as shown in Fig. 7, 2D site effects cannot extend to the whole surface area of a broad shallow basin, but are limited to an area close to the edges. It is thus imperative to pinpoint the width of this close-to-edge region *X* (Fig. 6). This close-to-edge region is referred to as "influential area" hereafter.

The widths *X* of the influential areas of these 50 basin configurations are derived from the $\overline{SAG}$ *(x/L)* (Fig. 7). And then the variations of *X* versus $v_{s,30}$ and *H* ($v_s$=800 m/s) are illustrated in Fig. 9 (a) and (b) respectively. Fig. 9 indicates that the width of the influential area *X* is more correlative to *H* ($v_s$=800 m/s) than to $v_{s,30}$. A linear fit can be derived from Fig. 9 (b):

$$X = 5H(v_s = 800) + 200 \tag{7}$$

where X- width of the influential area; $H(v_s=800)$- the depth of the top of the first layer with shear wave velocity greater than 800 m/s

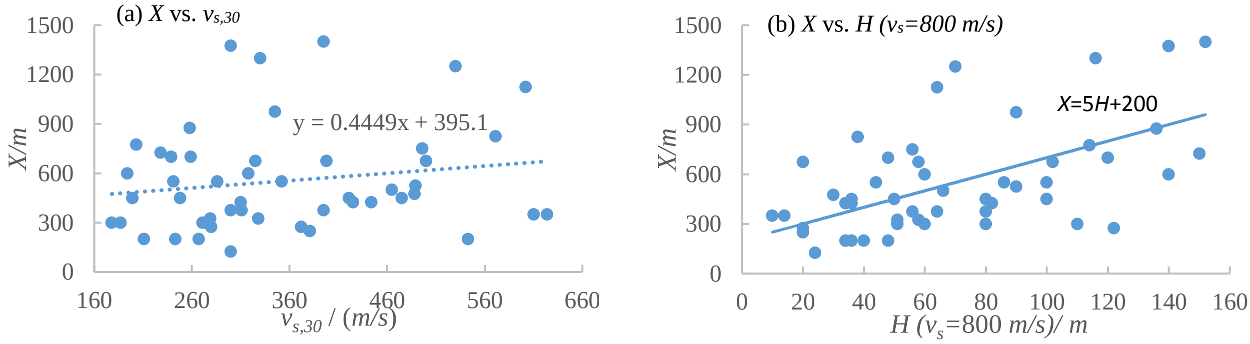


**Fig. 9** Influential area ***X*.** (a) *X* vs. $v_{s,30}$ ; (b) *X* vs. *H* *($v_s$=800 m/s)****.*** $H(v_s=800)$ denotes the depth of the top of the first layer with shear wave velocity greater than 800 m/s; $v_{s,30}$ is the average shear wave velocity of the topmost soil layers within 30m.

## 4.4 $\overline{SAG}$

The width of the influential area can be approximated by the Eq. (7). It is reasonable to only adjust the acceleration spectra of locations within the influential area, thus another indicator $\overline{SAG}$ is proposed to be the average value of $\overline{SAG}$ *(x/L)* within the influential area, namely in the range of -1 < *x/L* ≤ -*X/L* :

$$\overline{SAG} = average\left[\overline{SAG}\left(-1 < x/L \le -X/L\right)\right] \tag{8}$$

$\overline{SAG}$s and its values within one standard deviation ($\sigma$) are illustrated against $v_{s,30}$ and *H* *($v_s$=800 m/s)* in Fig. 10 (a) and (b) respectively. The $\overline{SAG}$ stays nearly constant with the increase in both $v_{s,30}$ and *H* *($v_s$=800 m/s)*, which indicates that the $\overline{SAG}$ is independent of both parameters. The $\overline{SAG}$*s* of these 50 basin models range from 1.1 to 1.6 with a mean value of 1.3, and are normally distributed as shown in Fig. 11. The 16th percentile, median and 84th percentile values are 1.2, 1.3 and 1.5 respectively.

Therefore, for a shallow basin, it is proposed to calibrate the acceleration spectra of locations only within the close-to-edge area with a width from the edge:

$$X = 5H(v_s = 800) + 200$$

by a factor of:

$$\overline{SAG} \in [1.2, 1.5]$$

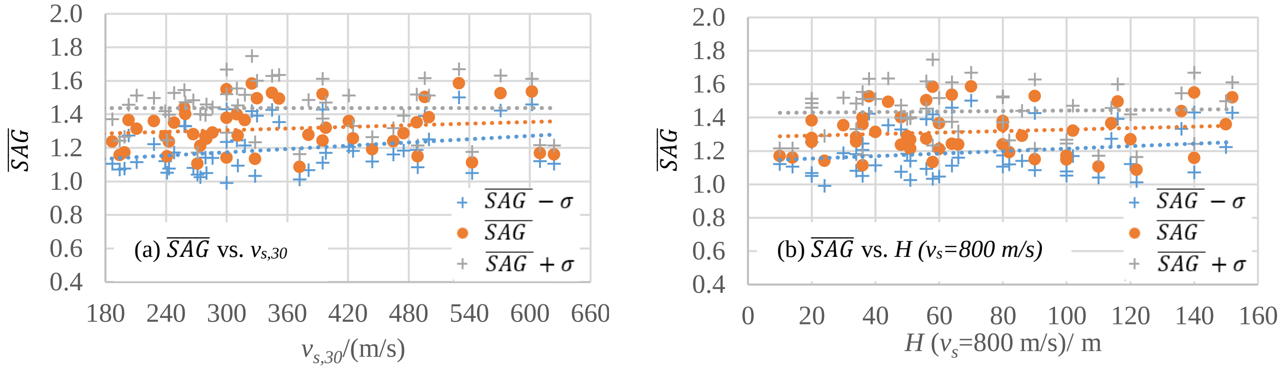


**Fig. 10** $\overline{SAG}$. (a) $\overline{SAG}$ vs. $v_{s,30}$ ; (b) $\overline{SAG}$ vs. *H (v*$_s$*=800 m/s)*. *H*($v_s$=800 m/s) denotes the depth of the top of the first layer with shear wave velocity greater than 800 m/s; $v_{s,30}$ is the average shear wave velocity of the topmost soil layers within 30m.

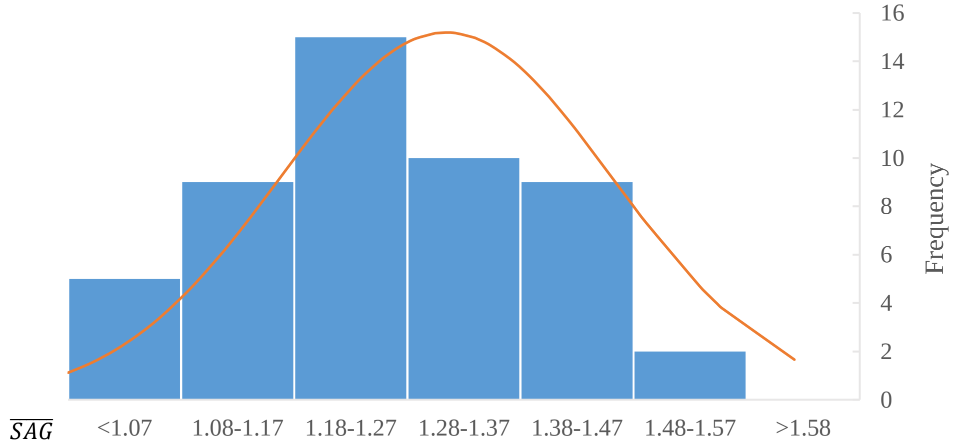


**Fig. 11** Histogram of the $\overline{SAG}$

## 4. Conclusion

With the aim of contributing to quantify the 2D sites of shallow basins, statistics-based numerical study was undertaken in this investigation. Vertically heterogeneous models were configured based on either real or hypothetic 1D soil profiles, it can be concluded that for a shallow basin, calibration to the acceleration spectra is only needed to locations within the close-to-edge region with a width around five times its depth by a factor ranging from 1.2 to 1.5.

## 5. Acknowledgements

This study is sponsored by the China Scholarship Council and the Queensland University of Technology (QUT). The first author would like to acknowledge their supports for this research, and the Pacific Earthquake Engineering Research Center (PEER) for the strong ground motions as well as the KiK-net database for the 1D soil profiles, and at the same time express his sincere gratitude to Prof. Pitilakis K. and Dr. Riga E. (Aristotle University of Thessaloniki, Greece) for their provision of the simulation code, Prof. Chávez-García F.J. (National Autonomous University of Mexico, Mexico) for his face-to-face discussions with the first author on this research, and the assistance of Prof. Bard P.Y. (University Joseph Fourier-Grenoble, France) and Prof. Faccioli E. (Italy) via email.

## 6. Reference

Aki K, Larner KL (1970) Surface motion of a layered medium having an irregular interface due to incident plane SH waves, J Geophys Res 75: 933-954

Bard PY, Bouchon M (1980a) The seismic response of sediment-filled valleys. Part 1. The case of incident SH waves, Bull Seismol Soc Am 70 (4):1263-1286

Bard PY, Bouchon M (1980b) The seismic response of sediment-filled valleys. Part 2. The case of incident P and SH waves, Bull Seismol Soc Am 70 (5):1921-1941

Bard PY, Bounchon M (1985) The two-dimensional resonance of sediment-filled valleys, Bull Seismol Soc Am 75 (2):519-541

Chávez-García FJ, Faccioli E (2000) Complex site effects and building codes: making the leap. J Seismol, 4:23–40

Ermert L, Poggi V, Burjanek J, Fah D (2014) Fundamental and higher two-dimensional resonance modes of an Alpine valley. Geophs J Int 198: 795-811

Gao S, Liu H, Davis PM, Knopoff L (1996) Localized Amplification of Seismic Waves and Correlation with Damage due to the Northridge Earthquake: Evidence for Focussing in Santa Monica. Bull Seism. Soc. Am. 86: S209-S230

Hanks TC (1975) Strong ground motion of the San Fernando, California, earthquake: Ground displacements, Bull Seism Soc Am 65, 1, 193-225

Hong TL, Helmberger DV (1978) Glorified optics and wave propagation in nonplanar structure. Bull Seismol Soc Am 68:1313–1330

Hudson JA (1962) The Total Internal Reflection of SH Waves. Geophys J Royal Astr Soc 6: 509-531

Hudson JA (1963) SH Waves in a Wedge-shaped Medium. Geophys J Royal Astr Soc 7 (5): 517-546

Ishii H, Ellis RE (1970a) Multiple reflection of plane SH waves by a dipping layer. Bull Seism Soc Am 60(1): 15-28.

Ishii H, Ellis RE (1970b) Multiple Reflection of Plane P and SV Waves By a Dipping Layer. Geophys. J. Royal Astr Soc 20: 11-30

Kawase H (1996) The cause of the damage belt in Kobe: ‘‘The basin-edge effect’’, constructive interferenceof the direct S-wave with the basin induced diffracted/Rayleigh waves. Seismol Res Lett 67(5):25–34

Khanbabazadeh H, Iyisan R (2014) A numerical study on the 2D behaviour of the single and layered clay basins. Bull Earthqe Eng 12(4):1515–1537

King JL, Tucker BE (1984) Observed variations of earthquake motion over a sediment-filled valley, Bull Seism Soc Am 74, 137-152

Kristek J, Moczo P, Archuleta RJ (2002). Efficient methods to simulate planar free surface in the 3D 4th-order staggered-grid finite-difference schemes, Studia Geophys Geod. 46, 355-381.

Kristek J, Moczo P (2003). Seismic wave propagation in viscoelastic media with material discontinuities–a 3D 4th-order staggered-grid finite-difference modelling, Bull Seism Soc Am, 93, 2273-2280.

Ktenidou OJ (2010) Experimental and theoretical study of seismic ground motion in the city of Aegion, Greece, focusing on local site and topography effects. PhD Thesis dissertation, Aristotle University of Thessaloniki, Greece

Ktenido OJ, Chávez-García FJ, Raptakis D, Pitilakis KD (2016). Directional dependence of site effects observed near a basin edge at Aegion, Greece. Bull Earthq Eng 14:623–645

Makra K, Chávez-García FJ (2016) Site effects in 3D basins using 1D and 2D models: an evaluation of the differences based on simulations of the seismic response of Euroseistest. Bulletin of Earthquake Engineering, DOI 10.1007/s10518-015-9862-7

Moczo P, Kristek J, Galis M ( 2004) Simulation of planar free surface with near-surface lateral discontinuities in the finite-difference modeling of seismic motion. Bull. Seism. Soc. Am. 94, 760-768.

Moczo P, Kristek J, Galis M, Pazak P, Balazovjech M (2007). The Finite-Difference and Finite-Element Modeling of Seismic Wave Propagation and Earthquake Motion, Acta Physica Slovaca 57, 177-406.

Papageorgiou AS, Pei D (1994) 3-D Response of Cylindrical Valleys of Arbitrary Cross-Section to Seismic Waves Incident from any Azimuthal Direction. *Proc 5th US Nat Conf on Earthquake Eng*, Chicago. Vol III: 45-54

Raptakis D, Makra K, Anastasidis A, Pitilakis (2004) Complex Site Effects in Thessaloniki (Greece): II. 2D SH Modelling and Engineering Insights. Bull Earthq Eng 2: 301-327

Riga E (2015) New elastic spectra, site amplification factors and aggravation factors for complex subsurface geology, towards the improvement of EC8. PhD Thesis dissertation, Aristotle University of Thessaloniki, Greece

Roten D, Fah D, Cornou C, Giardini D (2006) Two-dimensional resonances in Alpine valleys identified from ambient vibration wavefields. Geophs J Int 165: 889-905

Sánchez-Sesma FJ, Velazquez SA (1987) ON THE SEISMIC RESPONSE OF A DIPPING LAYER. Wave Motion, 9: 387-391

Trifunac MD (1971) Surface motion of a semi-cylindrical alluvial valley for incident plane SH waves, Bull Seism Soc Am 61:1755-1770

Trifunac MD, Lee VW (1978) Dependence of the Fourier amplitude spectra of strong motion acceleration on the depth of sedimentary deposits, Report No. CE 78-14, University of Southern California, Civil Engineering Department

Tucker BE, King JL (1984) Dependence of sediment-filled valley response on input amplitude and valley properties, Bull Seism Soc Am 74, 153-166

Vessia G, Russo (2013). Relevant features of the valley seismic response: the case study of Tuscan Northern Apennine sector. Bull Earthq Eng 11: 1633-1660

Wirgin A (1995) Resonant Response of a Soft Semi-Circular Cylindrical Basin. Bull Seism Soc Am 85 (1): 285-299

Wong TL, Trifuna MD (1974) Surface motion of a semi-elliptical alluvial valley for incident plane SH waves, Bull Seism Soc Am 64:1389-1408

Zhu C, Thambiratnam D, Zhang J (2015). Response of sedimentary basin to obliquely incident SH waves. Bull Earthq Eng, DOI 10.1007/s10518-015-9856-5

Zhu C, Thambiratnam D (2016). Interaction of geometry and mechanical property of trapezoidal sedimentary basins with incident SH waves, Bull Earthq Eng, DOI 10.1007/s10518-016-9938-z